The Sensitivity and Specificity of Susceptibility Weighted Imaging Phase (Swip) in Detecting Intracranial Large Artery Calcium Stenosis Compared to Cone Beam CT

Tawfiq Yousef Tawfiq Zyoud[1], Muhammad Hasif Bin Kamaruddin[1], Suzana Ab Hamid[1], Mohamad Syafeeq Faeez Bin Md Noh[1],Umar Ahmad[2], Abubakar Kabeer[3], Saiful Nizam Abdul Rashid[4], Subapriya Suppiah[1], Rozi Mahmud[1], Ezamin Abdul Rahim[1]

[1]*Department of Imaging, Faculty of Medicine and Health Sciences, University Putra Malaysia, 43400 Serdang,Selangor, Malaysia*
[2]*Department of Anatomy, Faculty of Basic Medical Sciences, Bauchi State University, PMB 65 Gadau, Nigeria*
[3]*Department of Human Anatomy, College of Medical Sciences, Federal University Lafia, P.M.B 146 Akunza, Lafia, Nasarawa State, Nigeria*
[4]*Ramsay Sime Darby Parkcity Medical Centre, 52200 Kuala Lumpur, Malaysia*

KEYWORDS

Intracranial calcification; SWI; CBCT; Intracranial atherosclerotic disease; Stroke.

ABSTRACT

Introduction: Intracranial calcifications are common and often associated with advanced stages of atherosclerosis. Studies estimating the prevalence of intracranial calcifications using other imaging modalities are common, however, studies comparing the diagnostic accuracies of cone-beam computed tomography (CBCT) and susceptibility-weighted imaging (SWI) and generated scoring systems for SWI are not well established. Aims: The objectives of the present study are to identify locations of intracranial calcifications; estimate the sensitivity and specificity rates for each intracranial vessel and each modality; estimate the sensitivity and specificity rates for diagnosing each grade of stenosis for each modality; and generate cutoff value for predicting each grade of intracranial stenosis and for each modality; as well as to develop a scoring system for estimating intracranial stenosis using SWI. Material and Methods: The study employs a prospective cross-sectional study design to collect brain data from 146 stroke patients who had initially undergone CBCT and SWI examinations. Data were collected using pro forma from January 2021 to December 2022 at Hospital Pengajar Universiti Putra Malaysia. Results: The results show an estimated prevalence of intracranial calcification of 87.7% and 92.5% for CBCT and SWI respectively. Regarding intracranial calcium grades, the prevalence of minimum – mild, moderate, and severe grade stenosis were 18.5%, 58,9%, and 10.3% respectively for CBCT and 2.7%, 33.8%, and 57.5% for SWI. Further, the results revealed that CBCT attained a sensitivity of 100% for the anterior cerebral artery, 71% for the middle cerebral artery, and 100% for the vertebral artery as well as a specificity of 90%, 80%, and 42% for the anterior cerebral artery, middle cerebral artery, and vertebral artery respectively. However, with the SWI modality, basilar, vertebral, and middle cerebral arteries reached a sensitivity of 90%, 63%, and 87% and a specificity of 82%, 95%, and 59%. Conclusion: In conclusion, both CBCT and SWI demonstrate reliable means of detecting intracranial calcifications and vessel stenosis with SWI outperforming CBCT.

1. Introduction

Intracranial atherosclerotic disease (ICAD) is a progressive pathological process that causes narrowing (stenosis) of the arteries in the brain. This narrowing can reduce blood flow to the brain, leading to cerebral hypoperfusion (inadequate blood supply to the brain) (Khan et al., 2011). ICAD is a major cause of stroke, myocardial infarction (heart attack), ischemic gangrene (tissue death due to lack of blood flow), and death worldwide (Bhatia et al., 2019; Shin et al., 2018). Multiple factors contribute to the development of ICAD, including lifestyle patterns, genetic predispositions, and larger burdens of hypertension (high blood pressure), diabetes mellitus (high blood sugar), and hyperlipidemia (high levels of lipids in the blood) (Bhatia et al., 2019; Yaghi et al., 2019). Important risk factors for ICAD include age, hypertension, diabetes mellitus, and metabolic syndrome (a cluster of risk factors for heart disease and stroke, including high blood pressure, high blood sugar, high cholesterol, and excess body fat) (Bang, 2014). Brain calcifications, which are deposits of calcium in the brain, have been reported in up to 72% of autopsy cases of ICAD (Jeng et al., 2010). Microscopic calcifications are the most common type of brain calcifications associated with ICAD. Calcification of the intracranial vasculature is an independent risk factor for stroke (Bang, 2014).

Cone beam computed tomography (CBCT) is an alternative imaging method that can be used for imaging of acute stroke and neurovascular pathologies such as large vessel occlusion (LVO) and intracranial atherosclerotic disease (ICAD) (Bang, 2014; Jeng et al., 2010).

CBCT images are produced by rotating the C-arm with a flat panel detector around in a 220-degree circular trajectory at the region of interest (ROI), which is the isocenter of the system (Jeng et al., 2010). The angiographic system will reconstruct three-dimensional (3D) volume images similar to CT images, thus providing the neuro-interventional radiologist with valuable information during the procedure (Ezzeddine et al., 2002; Kamran, 2015). Recent advances in angiographic systems and technology have enabled imaging capabilities with better contrast enhancement and superior spatial resolution to visualize anatomical structures in the intracranial region (Jeng et al., 2010).

Susceptibility Weighted Imaging (SWI) is an advanced MRI technique that exploits tissue magnetic susceptibility differences. It is susceptible to venous blood, hemorrhage, and mineralization, making it invaluable in neuroimaging for detecting microbleeds, vascular malformations, and brain iron deposition (Zyoud, Kabeer, Syafeeq, Noh, Binti, & Hamid, 2023)

Stroke is a leading cause of mortality and morbidity worldwide, including in Malaysia (Tan & Venketasubramanian, 2022). The most well-recognized biomarker to assess for future ischemic stroke risk attributable to ICAD is the degree of luminal stenosis as measured on angiography (Jeng et al., 2010). However, the composition of intracranial atherosclerotic plaque has largely been ignored in favor of luminal stenosis measurements (Jeng et al., 2010). Several documented pathologies of the brain are characterized by the presence of calcifications and hemorrhages, however, calcium is diamagnetic and, due to the presence of very few protons, makes it difficult to detect on conventional MR sequences (Chen et al., 2014; S. Wu et al., 2009).

The purpose of this study is to highlight the usefulness of cone-beam CT and susceptibility weighted imaging phase (SWIp) in detecting intracranial large artery calcium stenosis burden as well as their sensitivity and specificity in comparison.

2. Methodology

Study design

This study employs a prospective cross-sectional design, conducted over four years from January 2022 to December 2023 at Hospital Pengajar Universiti Putra Malaysia (HPUPM). Data were collected at specific points during this period to analyze a range of variables in the patient population, providing a snapshot of the phenomena under study during these particular time frames. The selection of this design allowed for efficient data collection, comprehensive assessment, and the ability to identify associations between different variables within the population sample at HPUPM during the specified period. It should be noted, however, that while this design can highlight correlations, it does not necessarily establish causality. In alignment with ethical research standards, we acquired ethical approval from the Universiti Putra Malaysia's Ethics Committee for Research Involving Human Subjects (JKEUPM), under the reference number (JKEUPM-2022-011).

Study subjects

For this study, we conducted a prospective data collection from Cone Beam Computed Tomography (CBCT) imaging of brain stroke patients between January 2022 and December 2023. Every patient included in the study underwent a brain CBCT examination, with subject selection predicated on predefined criteria. Several modalities were employed to identify arterial stenoses and occlusions seen in Intracranial Artery Disease (ICAD). These modalities included CT angiography, MR angiography, and Digital Subtraction Angiography (DSA). Despite DSA's recognition as the gold standard for assessing stenosis severity, it demonstrated inferior sensitivity in determining plaque morphology

compared to CTA and MRA. Notably, DSA, due to its invasive nature, comes with procedural risks, including stroke and dissection. Given these factors, we utilized DSA as the gold reference standard in our research.

Selection criteria

Study participants will be chosen according to specific eligibility criteria. Only patients satisfying these predetermined criteria will form part of the study population. The criteria essentially bifurcate into two categories - inclusion and exclusion. The inclusion criteria identify eligible participants for the study, while the exclusion criteria outline conditions under which potential participants would be disqualified from the study.

Inclusion criteria

For this study, the following inclusion criteria were used:

1. Adult patients of a predefined minimum age, to exclude pediatric cases.
2. Patients who have undergone a brain Cone Beam Computed Tomography (CBCT) examination at the Hospital Pengajar Universiti Putra Malaysia (HPUPM) within the established study period.
3. Patients with clinical symptoms suggestive of a brain stroke or radiological evidence of the same.
4. Patients who are capable of and have given informed consent for participating in the study.
5. Patients who show a willingness to participate in the study and comply with the requirements.
6. Patients who display indications of Intracranial Atherosclerotic Disease (ICAD) or are clinically suspected of the same, based on medical history, symptoms, or initial diagnostic tests.
7. Patients who have not undergone any recent neurosurgical procedures that could interfere with the calcium scoring in ICAD.

Exclusion criteria

The following are the exclusion criteria applied in this study

1. Patients with a known or suspected pregnancy, given the potential radiation exposure from the Cone Beam Computed Tomography (CBCT) examination.
2. Patients with a history of or a high suspicion of an allergic reaction, particularly to contrast agents used in imaging studies.
3. Patients with contraindications to contrast media (e.g., renal failure or severe asthma).
4. Patients who have undergone any form of neurosurgery or interventional procedures in the brain before the study.
5. Patients with other concurrent severe neurological disorders, which could interfere with the assessment of ICAD.
6. Patients with non-atherosclerotic vascular diseases of the brain (e.g., vasculitis, Moyamoya disease).
7. Patients with any condition that might interfere with calcium scoring, such as intracranial calcifications not related to ICAD (e.g., brain tumors, infections, etc.).
8. Patients who are incapable of giving informed consent due to cognitive or other impairments.

Sampling techniques

In alignment with the available data from the hospital utilized for this study, a total of 195 eligible patients with definite stroke diagnoses have been identified. The data collection process will employ a proportional stratified sampling methodology to ensure adequate representation across different strata within this patient population. This strategy allows for the preservation of proportionality within the sample, mirroring the distribution of the overall population and enhancing the statistical reliability of the study findings. This same sampling method will also be applied when collecting data from the control group. The control group will be selected from the same hospital population, ensuring that the control and case groups are comparable and minimizing potential confounding factors related to demographic or environmental differences. It's important to note that the control group will be chosen based on the criteria that they do not have the condition under investigation but are otherwise similar to the patient group (**Figure 2.1**).

$$Sampeling\ proportion = \frac{Number\ of\ IS\ patients\ from\ the\ hospital}{\text{Total number of IS patients in the hospital}} \times Sample\ size$$

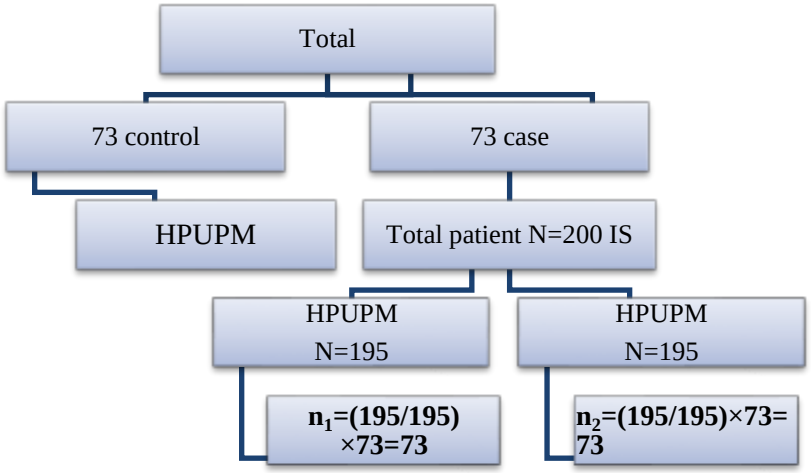

Figure 2.1: Illustration of sample size calculations for the study.

Data collection

The designated target population for this retrospective study consists of patients who have been diagnosed with ischemic stroke within the Radiology Departments of selected hospitals in Malaysia. The retrospective data were derived from the hospitals' Radiological Information Systems (RIS), which served as a comprehensive source of patient records and relevant clinical information. A specialized pro forma was employed to systematically extract and document this data from the RIS. It is important to note that this study involved no direct patient testing or additional sample collection beyond what was already available in the existing records.

The pro forma was designed to capture significant sociodemographic data, including patients' age, gender, weight, geographic region, and disease duration. Moreover, it facilitated the extraction of relevant medical imaging data, specifically the required Magnetic Resonance Imaging (MRI) scans. The pro forma also recorded pertinent clinical diagnoses associated with each patient's medical record.

Cone-Beam Computed Tomography

In this study, seventy-three patients presenting with acute stroke who underwent mechanical thrombectomy were evaluated. A baseline Cone Beam Computed Tomography (CBCT) was performed before the thrombectomy, and a post-procedural CBCT was conducted to identify any potential

bleeding or new infarct post-thrombectomy. All examinations were executed utilizing a bi-plane flat detector C-arm angiographic system (Philips AlluraClarity FD 20/15, Philips Medical System, Eindhoven, Netherlands).

Degree of calcification

In this study, calcium scoring was performed using non-contrast CT scans to detect and quantify vascular calcification. This was further corroborated by contrast-enhanced CT imaging to distinguish intraluminal calcification from adjacent bony structures. The Agatston method, performed on a dedicated workstation (Syngo, Siemens, Forchheim, Germany), was used to assess calcium scores. This method identifies a calcified plaque as a structure exhibiting radiodensity greater than 130 Hounsfield units (Hu) over an area of at least 1 mm^2.

Susceptibility weighted imaging

The MRI imaging for this study was conducted using a clinical 1.5 T MRI scanner (Philips Ingenia 1.5T MRI system, Malaysia), abiding by the standard departmental protocols. The Susceptibility Weighted Imaging (SWI) sequences were captured using specific parameters: Repetition Time (TR) set at 48 ms, Echo Time (TE) set at 40 ms, flip angle at 15 degrees, bandwidth at 80 kHz, slice thickness of 1.2 mm comprising 128 slices per slab, Field of View (FOV) at 146 x 180 mm, and matrix size at 256 x 512. The acquisition time was noted to be 4.57 minutes, utilizing an Integrated Parallel Acquisition Techniques (iPAT) factor of 2.

Diffusion-weighted images

Diffusion Weighted Imaging (DWI) maps in this study were formulated from diffusion tensor imaging (DTI) scans. We performed a single-shot spin-echo echo-planar imaging (EPI) axial DTI sequence, applying diffusion gradients along 20 orthogonal directions. We used an effective high b value of 1000 s/mm^2 for each of these 20 diffusion-encoding directions. Furthermore, a non-diffusion-weighted measurement (b=0 s/mm^2) was included in the imaging protocol.

Data analysis

Statistical Package for Social Sciences (SPSS V. 25, Inc., Chicago, IL, USA), R version 3.6.1, and MedCalc Statistical Software version 23.1.0 (MedCalc Software bvba, Ostend, Belgium; https://www.medcalc.org; 2021) was used for statistical data analysis. Collected data was checked for missing and incomplete data and then was entered into IBM SPSS statistics software version 26.0.

The initial step in our analysis involved an exploratory data assessment utilizing descriptive statistics such as frequency, mean, and standard deviation for all research variables, including socio-demographic characteristics. To substantiate the research hypotheses, we employ inferential statistical methods. Pearson/Spearman correlation coefficients, one-way repeated measures ANOVA, and independent-sample t-tests were used to compare the two methods under consideration and for comparing the case and control groups across all research variables, provided the data adheres to a normal distribution.

When the data deviated from the assumption of normal distribution, nonparametric methods, including the Friedman test and Mann-Whitney U-test for comparisons, as well as Spearman correlation for determining associations between research variables, were implemented.

The accuracy of the two methods was ascertained using the Relative Operating Characteristic (ROC) analysis, specifically evaluating sensitivity and specificity. Continuous data was represented as mean ± SD or median along with interquartile range (IQR), whereas categorical data will be presented as numbers (percentages).

To analyze risk factors, as well as the severity and location of cerebral artery atherosclerosis, we employ independent sample t-tests and Pearson's chi-square tests. Analysis of variance (ANOVA) was

employed to gauge differences across the groups, and histograms were generated to visualize the distribution of specific data sets. Any group differences were considered statistically significant when the p-value was less than 0.05.

3. Result and Discussion

Characteristics of Study Participants and Intercorrelations

A total of 146 (82 males and 64 females) participants aged 68.41 ± 11.26 years (range 42 – 87) were involved in this study. Descriptive statistics for intracranial large artery calcification area as identified by cone beam CT and susceptibility weighted imaging phase are provided in Table 4.1. Considering cone beam CT, the distribution of calcification of intracranial arteries differs significantly (χ^2 = 94.91, *P* <0.001). Regarding single-vessel intracranial vessel calcifications, the highest prevalence was observed within the lumen of the internal carotid artery (36.3%) followed by the basilar artery (17.1%). The prevalence observed for vertebral artery internal carotid artery and middle cerebral artery are respectively 12.3% and 9.6%. Internal carotid artery (ICA) and basilar artery (BA) had the least prevalence of calcification (2.7%).

The mean values of calcification area differed significantly across intracranial arteries (F = 6.92, *P* <0.001). The VA and ICA had the highest mean calcification area of 0.31 ± 0.2 followed by the basilar artery and internal carotid artery with a mean calcification area of 0.26 ± 0.07. The calcification areas of the basilar artery, vertebral artery, and internal carotid artery did not differ significantly (P >0.05) from those of the other arteries, but the calcification areas of the anterior cerebral artery, middle cerebral artery, basilar artery, and internal carotid artery differed significantly (P <0.05) from those of the other arteries.

A statistically significant inverse association was observed between chronological age and the middle cerebral artery (r = –0.82, *P* <0.001), basilar artery (r = –0.57, *P* <0.001), and the internal carotid artery (r = –0.96, *P* <0.001). Age and the anterior cerebral artery, vertebral artery, internal carotid artery, and vertebral and internal carotid artery do not attain a statistically significant correlation.

Table 3.1 also shows the distribution of intracranial artery calcifications according to severity ratings. By employing CBCT, it was observed that two-thirds (67.2%) of the patients had moderate-grade calcification areas, while 21.1% and 11.7% had minimum-med and severe-grade calcification areas, respectively. A statistically significant difference was shown by the chi-square test for differences in proportions across intracranial artery stenosis (χ2 = 67.70, P <0.001).

Utilizing the susceptibility-weighted imaging phase, the prevalence of calcification sites in intracranial arteries varied from 5.5% in the vertebral artery to 47.3% in the middle cerebral artery. Both modalities can detect intracranial calcifications within the lumen of the following vessels: internal carotid artery, middle cerebral artery, basilar artery, vertebral artery, and basilar artery may all be found to have calcification using both modalities. A chi-square test was used to test for differences in the proportions of intracranial arteries identified by both modalities. The results showed that the differences were not statistically significant (χ^2 = 0.19, *P* = 0.666).

A modest inverse association was found between age and the internal carotid artery (r = –0.49, *P* <0.05), while a higher inverse correlation was seen between the middle cerebral artery and the vertebral artery (r = –0.97, *P* <0.001). Overall, the findings showed an inverse association between age and intracranial calcification.

Table 3.1: Descriptive statistics and intercorrelation of key variables

Calcification Area	n	Mean ± SD	r (95% CI)	Min – Mild	Moderate	Severe
CBCT						
ACA	5	0.14 ± 0.01a	–0.21 (–0.92, 0.83)	5 (100.0%)	-	-

MCA	14	0.10 ± 0.12ab	–0.82 (–0.94, –0.50)**	8 (57.1%)	6 (42.9%)	-
BA	25	0.10 ± 0.09bc	–0.57 (–0.79, –0.23)**	4 (16.0%)	21 (84.0%)	-
VA	9	0.17 ± 0.13bc	0.12 (–0.59, 0.73)	2 (22.2%)	5 (55.6%)	2 (22.2%)
ICA	53	0.19 ± 0.22bc	–0.21 (–0.45, 0.07)	5 (9.4%)	37 (69.8%)	11 (20.8%)
VA and ICA	18	0.31 ± 0.20bc	0.08 (–0.40, 0.53)	3 (16.7%)	13 (72.2%)	2 (11.1%)
BA and ICA	4	0.26 ± 0.07c	–0.96 (–1.00, 0.08)**	-	4 (100.0%)	-
	128	**F = 6.92, P < 0.001**		**27 (21.1%)**	**86 (67.2%)**	**15 (11.7%)**
SWIp						
MCA	69	0.50 ± 0.46d	–0.01 (–0.24, 0.24)	2 (2.9%)	26 (37.7%)	41 (59.4%)
BA	10	0.10 ± 0.09a	0.26 (–0.45, 0.76)	-	1 (11.1%)	8 (88.9%)
VA	8	0.15 ± 0.18ab	0.17 (–0.61, 0.78)	2 (25.0%)	-	6 (75.0%)
ICA	18	0.27 ± 0.10cd	0.49 (0.03, 0.78)*	-	6 (33.3%)	12 (66.7%)
BA and ICA	11	0.17 ± 0.07abcd	0.10 (–0.53, 0.66)	-	4 (36.4%)	7 (63.6%)
MCA and VA	8	0.21 ± 0.05bcd	–0.97 (–0.99, –0.82)**	-	2 (25.0%)	6 (75.0%)
MCA and BA	11	0.19 ± 0.15abc	–0.38 (–0.80, 0.28)	-	6 (60.0%)	4 (40.0%)
	135	**F = 12.08, P < 0.001**		**4 (3.0%)**	**45 (33.8%)**	**84 (63.2%)**

Screening Effectiveness, Cutoff Points, Sensitivities, and Specificities of CBCT and SWIP for Detecting Intracranial Artery Calcification Areas

The diagnostic accuracies of SWI and cone beam CT to accurately detect intracranial artery calcification were evaluated using the area under the curve (AUC). Table 3.2 presents an extension of the receiver operating characteristic (ROC) curve analysis by summarizing the sensitivity, specificity, positive predictive value, and negative predictive value along with their 95% confidence intervals, as derived from the analyses of ROC curves of calcification areas of each intracranial artery using both imaging modalities (CBCT and SWIp). Each of the ROC curves depicts the balance between sensitivity and specificity. The corresponding ROC curves are presented in Figures 3.1 to 3.4.

In the case of cone beam CT, in general, the area under the receiver operating characteristic curve for vertebral artery, anterior cerebral artery, middle cerebral artery, vertebral and internal carotid artery were significantly larger than 0.5, while the area under the receiver operating characteristic curve for basilar and internal carotid arteries did not differ significantly ($P > 0.05$) from 0.5. Additionally, the area under the receiver operating characteristic curves for predicting severity grades differs significantly ($P > 0.05$) from 0.5.

The accuracy level of CBCT for identifying calcification in the anterior cerebral artery as assessed by the area under the curve was estimated to be 0.98 (95% CI 0.93 to 0.99) and was statistically

significantly different (P <0.001) from 0.5, with a Youden index of 0.90. It was observed that the calcification area of ≤0.01 performed as the best optimal cut-off point to detect calcification in the anterior cerebral artery with sensitivity, specificity, negative predictive value, and positive predictive values of 100, 90, 99, and 29% respectively. The AUC signifies excellent predictive significance of the cut-off point. The ROC curve is presented in Figure 3.1.

Regarding the middle cerebral artery, the accuracy level of CBCT for identifying calcification using the area under the ROC curve was 0.70 (95% CI 0.61 to 0.77) and significantly differed from 0.5 (P = 0.024) with a Youden index of 0.52. The best-performing cut-off was calcification area ≤0.14 with corresponding sensitivity, specificity, negative predictive value, and positive predictive value of 71, 80, 96, and 30% respectively. The AUC suggests good diagnostic ability of the cut-off point to diagnose intracranial calcification in the middle cerebral artery. The corresponding ROC curve is presented in Figure 3.1. The optimal cut-off to detect calcification in the basilar artery was ≤0.82 with corresponding sensitivity, specificity, negative predictive value, and positive predictive value of 88, 49, 94, and 29% respectively. The AUC for the basilar artery was calculated to be 0.59 (95% CI 0.50 to 0.67) and did not differ significantly from 0.5 (P = 0.093) and the corresponding ROC curve is shown in Figure 3.1. The area under the ROC curve analysis of the vertebral artery was 0.64 (95% CI 0.56 to 0.72) and differed significantly from 0.5 (P = 0.023), indicating good diagnostic ability. The Youden index was estimated at 0.42. Based on the findings of ROC curve analysis, the calcification area cut-off to detect calcification in the vertebral artery was estimated as > 0.04 with commensurate sensitivity, specificity, negative predictive value, and positive predictive value of 100, 42, 99, and 10% respectively. Figure 4.1 depicts the ROC curve for the vertebral artery. The area under the curve of the internal carotid artery was the lowest 0.55 (95% CI 0.46 to 0.64) compared to all the other intracranial arteries and did not differ from 0.5 (P = 0.348). This indicates the inability of the cut-off point to discriminate between calcified internal carotid artery from normal. Its ROC curve is depicted in Figure 3.1.

Moreover, in the case of the vertebral artery and internal carotid artery, the area under the ROC curve was estimated to be 0.72 (95% CI 0.63 to 0.79) and was significantly different from 0.5 (P = 0.007) while the Youden index was 0.49. It was observed that a calcification area of > 0.29 performed as the best optimal cut-off point to diagnose calcification in the vertebral and internal carotid arteries with sensitivity, specificity, negative predictive value, and positive predictive value of 61, 88, 93, and 44% respectively. The ROC curve is depicted in Figure 3.1.

The order of diagnostic accuracy of cone beam CT in diagnosing intracranial vessel calcification is anterior cerebral artery > vertebral and internal carotid artery > middle cerebral artery > vertebral artery based on the area under the ROC curve. Based on sensitivity, the order of diagnostic accuracy of cut-off points indicated that the anterior cerebral artery and vertebral artery have perfect sensitivity (100%), followed by the middle cerebral artery.

In the case of the accuracy of susceptibility weighted imaging phase in identifying intracranial calcification and degree of stenosis as assessed by area under the curve, the sensitivity, specificity, positive predictive value, and negative predictive value along with their 95% confidence intervals, as derived from the analyses of ROC analyses were also summarized in Table 3.2 and their corresponding ROC curve is presented in Figure 4.3. Regarding the basilar artery, the area under the ROC curve was estimated to be 0.85 (95% CI 0.78 to 0.91) significantly different from 0.5 (P <0.001), and has a Youden index of 0.72. It was further observed that an intracranial calcification area of ≤0.13 performed as the best optimal cut-off value to detect calcification in the basilar artery, with sensitivity, specificity, negative predictive value, and positive predictive values of 90, 82, 99, and 28% respectively. The corresponding ROC curve is depicted in Figure 3.3.

As regards the basilar artery and internal carotid artery, its area under the curve is estimated as 0.70 (95% CI 0.62 to 0.78) and intriguingly, significantly different from 0.5 (P <0.001) with a Youden index estimated as 0.49. The basilar artery and internal carotid artery cut-off value for intracranial calcification was calculated to be ≤0.28, with sensitivity, specificity, negative predictive value, and

positive predictive value of 100, 49, 99, and 14% respectively. For the internal carotid artery, the area under the curve was not statistically different from 0.5 (P = 0.388). This shows that both modalities (CBCT vs. SWIp) showed low diagnostic power to identify calcification in the internal carotid artery.

The optimal cut-off to detect calcification in the middle cerebral artery was > 0.18 with a Youden index of 0.46. The area under the ROC curve was estimated to be 0.78 (95% CI 0.70 to 0.85) and significantly different from 0.5 (P <0.001). The sensitivity, specificity, negative predictive value, and positive predictive value were calculated as 87, 59, 82, and 68% respectively. The area under the ROC curve for the middle cerebral artery and basilar artery did not differ from 0.5 (P = 0.124).

Overall, the area under the curve values for SWIp was highly significant for the basilar artery, vertebral artery, middle cerebral artery, basilar artery internal carotid artery middle cerebral artery, and vertebral artery, indicating high accuracy of SWIp to detect calcification.

4.2.1 Evaluation of Intracranial Artery Stenosis

The diagnostic accuracy of cone beam CT to assess the severity grade of calcification was also assessed by the area under the curve. The sensitivity, specificity, negative predictive value, and positive predictive value along with their 95% confidence intervals derived from the analyses of the degree of severity of intracranial artery stenosis were also presented in Table 3.2. From Table 3.1, there are a limited number of patients with minimum – mild and severe degrees of stenosis. Consequently, the accuracy levels of both modalities for identifying severity grades of intracranial stenosis per intracranial artery as assessed by area under the curve were not performed. Rather, the degrees of stenosis for the combined intracranial arteries were assessed.

All the areas under the curve for predicting severity grades for both modalities were significantly different from 0.5 for both modalities (Figure 3.2 and Figure 3.4). Cone beam CT performed best in detecting a minimum – mild degree of stenosis followed by a moderate degree of stenosis as assessed by the area under the curve. Using CBCT as the diagnostic measure for the level of severity gave an area under the ROC curve of 0.84 (95% CI 0.76 to 0.89), 0.76 (95% CI 0.68 to 0.82), and 0.73 (95% CI 0.65 to 0.80) for minimum – mild, moderate and severe level of stenosis respectively (Figures 3.2). The optimum cut-off points for predicting minimum – mild degree of stenosis, with calcification area of ≤0.17 were observed to have a sensitivity, specificity, negative predictive value, and positive predictive value of 86, 65, 94, and 40% respectively. The cut-off value of the calcification area for identifying a moderate degree of stenosis was calculated to be > 0.02 with a Youden index of 0.53. Severe level of intracranial stenosis had the highest sensitivity (100%) whereas moderate degree of stenosis had the lowest specificity (60%) for detecting stenosis.

Regarding severity grades of the intracranial arteries using SWIp, the optimal cut-off values vary from 0.21 to 0.45 for all the intracranial arteries in this study (Figure 3.4). Minimum – mild severity grade had the largest area under the curve. With regards to a minimum – -mild grade, the area under the ROC curve was estimated to be 0.83 (95% CI 0.76 to 0.89), and the Youden index was 0.63. It was observed that a calcification area of <0.39 performed as the best optimal cut-off point to detect minimum – mild severity grade, with sensitivity, specificity, negative predictive value, and positive predictive value of 86, 61, 94, and 36% respectively.

Furthermore, all the negative predictive values of intracranial artery calcification areas in this study were more than the positive predictive values, suggesting that the modalities were suitable for excluding a population of individuals without intracranial artery calcification from a population of patients with intracranial artery calcification. The study also found that SWI has better discriminatory power to detect intracranial artery calcification in the basilar artery and middle cerebral artery than cone beam CT. On the other hand, cone beam CT was observed to have better discriminatory power to detect intracranial artery calcification in the anterior cerebral artery than its SWI counterpart.

Table 3.2: AUCs, optimal cut-off values, SN, SP, NPV, and PPV of CBCT and SWIp in ROC analysis for predicting intracranial artery calcification

CBCT	AUC (95% CI)	P	YI	CP	SN (95% CI)	SP (95% CI)	NPV (95% CI)	PPV (95% CI)
ACA	0.98 (0.93, 0.99)	<0.001	0.90	≤0.01	100 (48, 100)	90 (84, 95)	99 (98, 100)	29 (20, 42)
MCA	0.70 (0.61, 0.77)	0.024	0.52	≤0.14	71 (42, 92)	80 (72, 87)	96 (91, 98)	30 (21, 42)
BA	0.59 (0.50, 0.67)	0.093	0.37	≤0.82	88 (69, 98)	49 (39, 59)	94 (85, 98)	29 (24, 34)
VA	0.64 (0.56, 0.72)	0.023	0.42	> 0.04	100 (66, 100)	42 (34, 51)	99 (98, 100)	10 (9, 12)
ICA	0.55 (0.46, 0.64)	0.348	0.17	> 0.03	85 (72, 93)	32 (22, 44)	76 (60, 87)	46 (42, 51)
VA and ICA	0.72 (0.63, 0.79)	0.007	0.49	> 0.29	61 (36, 83)	88 (80, 93)	93 (89, 96)	44 (30, 59)
Min – Mild	0.84 (0.76, 0.89)	<0.001	0.56	≤0.17	86 (67, 96)	65 (55, 74)	94 (87, 98)	40 (33, 47)
Moderate	0.76 (0.68, 0.82)	<0.001	0.53	> 0.02	99 (94, 100)	54 (41, 67)	97 (82, 100)	76 (71, 81)
Severe	0.73 (0.65, 0.80)	<0.001	0.60	> 0.07	100 (78, 100)	60 (51, 68)	99 (98, 100)	22 19, 26)

Pairwise Comparative Analysis of Diagnostic Ability of CBCT and SWIp

A comparative analysis of the area under the curve for the basilar artery and middle cerebral artery showed that the attained area under the curve assessed using SWIp was significantly different and superior to that of the area under the curve of its cone beam CT counterpart (Table 3.3). The difference between areas under the curve is 0.29 ((95% CI 0.13 to 0.44), P <0.001) for the basilar artery and 0.19 (95% CI 0.02 to 0.36), P = 0.025) for the middle cerebral artery. The area under the curve of vertebral artery using cone beam CT was not significantly different from the area under the curve for SWIp (difference in curve areas = 0.10 (95% CI –0.13 to 0.33), P = 0.403). Additionally, the area under the curve for detecting minimum – mild and moderate-grade stenosis was significantly different between cone beam CT and SWIp. Cone beam CT showed more superior ability to detect minimum – mild and moderate grade stenosis than SWIp. The difference in curve areas for minimum – mild grade is 0.17 ((95% CI 0.05 to 0.28), P = 0.004) while the difference in curve areas for moderate grade is 0.19 ((95% CI 0.06, 0.32), P = 0.003). The area under the curve for severe grade intracranial calcium stenosis using cone beam CT was not significantly different from that of SWIp. The difference in curve areas was found to be 0.01 ((95% CI –0.11 to 0.14), P = 0.825).

Table 3.3: Pairwise comparison of ROC curves for identification of intracranial artery calcification

Variables	Diff. AUC (95% CI)	SE	*P*-value
Basilar artery	0.29 (0.13, 0.44)	0.08	**<0.001**
Middle cerebral artery	0.19 (0.02, 0.36)	0.09	**0.025**
Vertebral artery	0.10 (–0.13, 0.33)	0.12	0.403
Min – Mild	0.17 (0.05, 0.28)	0.06	**0.004**
Moderate	0.19 (0.06, 0.32)	0.07	**0.003**
Severe	0.01 (–0.11, 0.14)	0.06	0.825

Diagnostic Accuracy of SWIp Compared to CBCT

The diagnostic accuracy of SWIp to assess intracranial artery calcification using conventional cone beam CT compared to SWIp is presented in Table 3.4. Considering the basilar artery, the diagnostic accuracy of SWIp to detect calcification using conventional CBCT was 84.2% (95% CI 77.3 to 89.7), indicating that only a few patients were misclassified (15.8%). The sensitivities and specificities of using SWIp to assess intracranial artery calcification area considering conventional CBCT were also presented in the table. The results revealed high sensitivity of SWIp in detecting calcification in the middle cerebral artery and high specificity for the basilar artery. In contrast, the diagnostic accuracy of SWIp to detect calcification of the middle cerebral artery is comparatively lower 62.3% (95% CI 53.9 to 70.2) than that for the basilar artery.

Intra-Observer Agreement

Table 3.5 presents the results of intra-observer agreement on calcification areas between SWIp and conventional cone beam CT. An intra-class correlation coefficient (ICC) of 0.88 (95% CI 0.26 to 0.99) was observed between CBCT and SWIp for the basilar artery, indicating high inter-rater reliability. A near moderate inter-rater reliability was observed between both modalities for the middle cerebral artery with an ICC of 0.48 (95% CI 0.27 to 0.82). A much lower inter-rater agreement was noticed between both modalities for the internal carotid artery and vertebral artery with ICC of 0.25 (95% CI 0.31 to 0.66) and 0.34 (95% CI 0.15 to 0.95) respectively. The extent of agreement between both modalities for assessing calcification areas was also evaluated using linear regression models (Figure 3.5). Results of the linear regression analysis revealed that a linear relationship in calcification areas of basilar artery as measured by CBCT and SWIp could be expressed by the following equation CBCT = 0.05 + 0.11*SWIp (Figure 3.5). Additionally, a statistically significant linear relationship in the calcification areas between CBCT and SWIp was established from the high Pearson's correlation coefficient (r = 0.88, 95% CI 0.26 to 0.99) for calcification area of the basilar artery as assessed by CBCT and SWIp. Results of the regression analysis for the basilar artery, middle cerebral artery, internal carotid artery, and vertebral artery are depicted in Figure 3.5.

McNemar's test was used to test for significant differences in measurements of intracranial artery calcification area as assessed by both modalities (CBCT and SWIp). Results of McNemar's test revealed a statistically significant difference between CBCT and SWIp for measuring basilar artery and middle cerebral artery whereas, no significant difference was observed between both modalities for assessing intracranial artery calcification of internal carotid artery and vertebral artery.

Results for Bland–Altman analysis showing bias and limits of agreement (LOA) (defined as mean difference ± 1.96 x standard deviation of the differences) between CBCT and SWIp are given in Table 3.5 and the corresponding plots are shown in Figure 3.5. The bias for the four intracranial arteries ranges from -0.38 to 0.03. The Bland-Altman analysis showed a mean bias between both modalities for the basilar artery as -0.03 (-0.08, 0.03) with LOA of -0.19 to 0.14.

Diagnostic Test Accuracy of SWIp Scoring System for Large Artery Calcium Stenosis

Table 3.6 and the corresponding Figure 4.6 present a modeled scoring system for large calcium stenosis of susceptibility weighted imaging phase. Except for patients classified as not having intracranial artery stenosis, the area under the ROC curve for minimum – mild, moderate, and severe stenosis were identified as significantly different from 0.5 (P <0.001). The optimal SWIp cut-off to detect null severity was ≤ 845. The area under the curve was 0.60 (95% CI 0.51, 0.68), Youden index of 0.25. The area under the curve was not significantly different from 0.5 (P = 0.177). In the case of minimum – mild grade stenosis, the area under the ROC curve was estimated to be 0.96 (95% CI 0.91 to 0.98) and the Youden index was 0.87. It was observed that patients with a calcium score of ≤ 779 performed as the best optimal score to identify patients with minimal – mild stenosis with sensitivity, specificity, negative predictive value, and positive predictive value of 100, 87, 99, and 68% respectively. The commensurate ROC curve is presented in Figure 3.6b. Regarding moderate grade stenosis, it was observed that the best performing cut-off value was ≤ 620 with corresponding sensitivity, specificity, negative predictive value, and positive predictive value of 92, 73, 83, and 81% respectively. The ROC curve is depicted in Figure 3.6c. The area under the ROC curve ranged from 0.72 to 0.96 (P <0.001), suggesting good/excellent diagnostic ability of the new SWIp score to identify patients with minimum – mild to severe intracranial artery stenosis. At all severity grades, the negative predictive values were much higher than the positive predictive value, suggesting that the new SWIp scores were able to correctly exclude patients not within any severity grade of interest.

Table 3.4: Diagnostic accuracy of using SWIp as against CBCT

	Sensitivity (%)	Specificity (%)	Diagnostic accuracy (%)
BA	24.0 (9.4, 45.1)	96.7 (91.8, 99.1)	84.2 (77.3, 89.7)
MCA	100 (76.8, 100.0)	58.3 (49.4, 66.8)	62.3 (53.9, 70.2)
ICA	30.2 (18.3, 44.3)	97.8 (92.4, 99.7)	73.3 (65.3, 80.3)
VA	44.4 (13.7, 78.8)	97.1 (92.7, 99.2)	93.8 (88.6, 97.1)

Table 3.5: Accuracy and intra-class correlation of calcification area measurement using both modalities

Parameter	**Bias (95% CI)**	**LLOA (95% CI)**	**ULOA (95% CI)**	**ICC (95% CI)**	**r (95% CI)**	**P#**
BA	-0.03 (-0.08, 0.03)	-0.19 (-0.29, -0.08)	-0.14 (0.03, 0.24)	0.14 (0.03, 0.24)	0.85 (0.71, 0.98)	0.003
MCA	-0.38 (-0.49, -0.28)	-0.74 (-0.93, -0.56)	-0.03 (-0.21, 0.16)	0.48 (0.27, 0.82)	0.37 (0.28, 0.74)	<0.001
ICA	-0.08 (-0.15, 0.00)	-0.38 (-0.52, -0.25)	0.23 (0.09, 0.37)	0.25 (0.31, 0.66)	0.26 (0.27, 0.67)	0.317
VA	0.03 (-0.18, 0.25)	-0.46 (-0.84, -0.08)	0.53 (0.15, 0.91)	0.34 (0.15, 0.95)	-0.34 (-0.84, 0.48)	0.724

Table 3.6: Diagnostic test accuracy of SWIp scoring system for varying severity grades of large artery calcium stenosis

SWIp	**AUC (95% CI)**	**P**	**YI**	**CP**	**SN (95% CI)**	**SP (95% CI)**	**NPV (95% CI)**	**PPV (95% CI)**

None	0.60 (0.51, 0.68)	0.177	0.25	≤ 845	100 (79, 100)	25 (18, 34)	99 (94, 100)	15 (14, 17)
Min – mild	0.96 (0.91, 0.98)	<0.001	0.87	≤ 779	100 (88, 100)	87 (79, 93)	99 (93, 100)	68 (55, 78)
Moderate	0.85 (0.78, 0.91)	<0.001	0.65	≤ 620	92 (83, 97)	73 (60, 84)	83 (72, 90)	81 (73, 86)
Severe	0.72 (0.64, 0.80)	<0.001	0.57	≤ 524	100 (78, 100)	57 (48, 66)	99 (91, 100)	22 (18, 26)

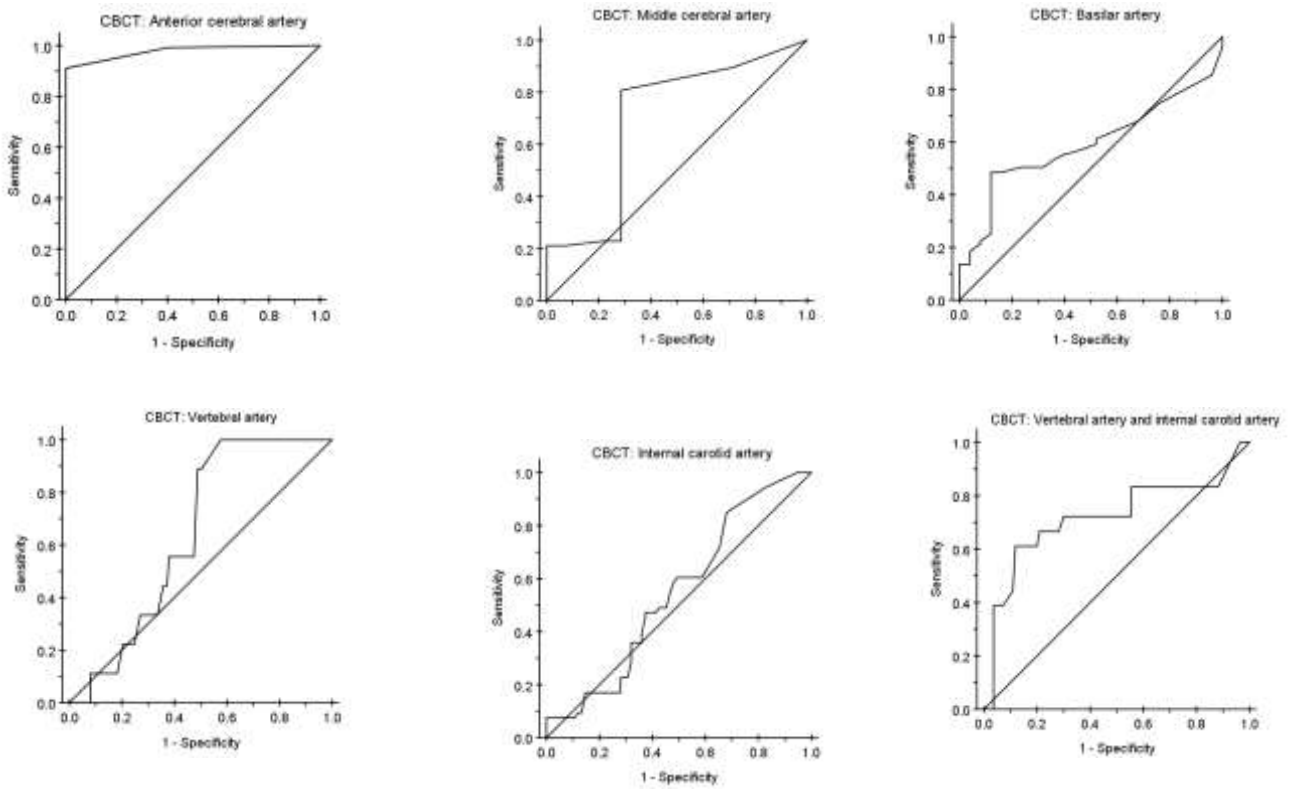

Figure 3.1: Receiver operating characteristic curve of cone beam CT to identify intracranial arteries calcification. The 45° (reference) the line represents chance as a diagnostic criterion (AUC = 0.5).

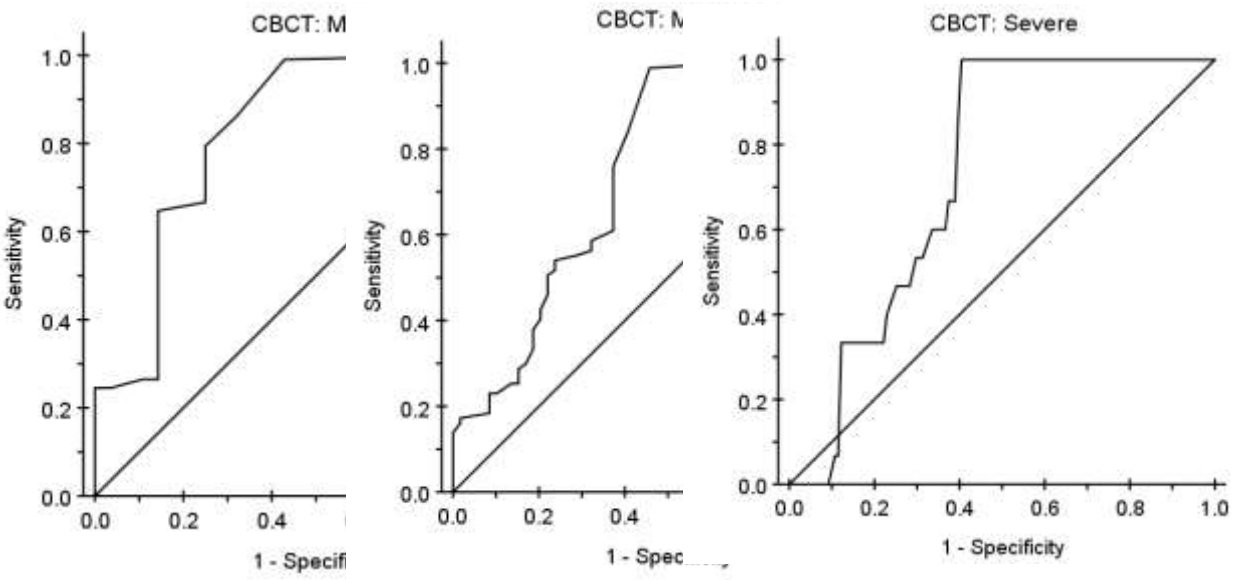

Figure 3.2: Receiver operating characteristic curve of cone beam CT to identify intracranial arteries stenosis. The 45° (reference) the line represents chance as a diagnostic criterion (AUC = 0.5).

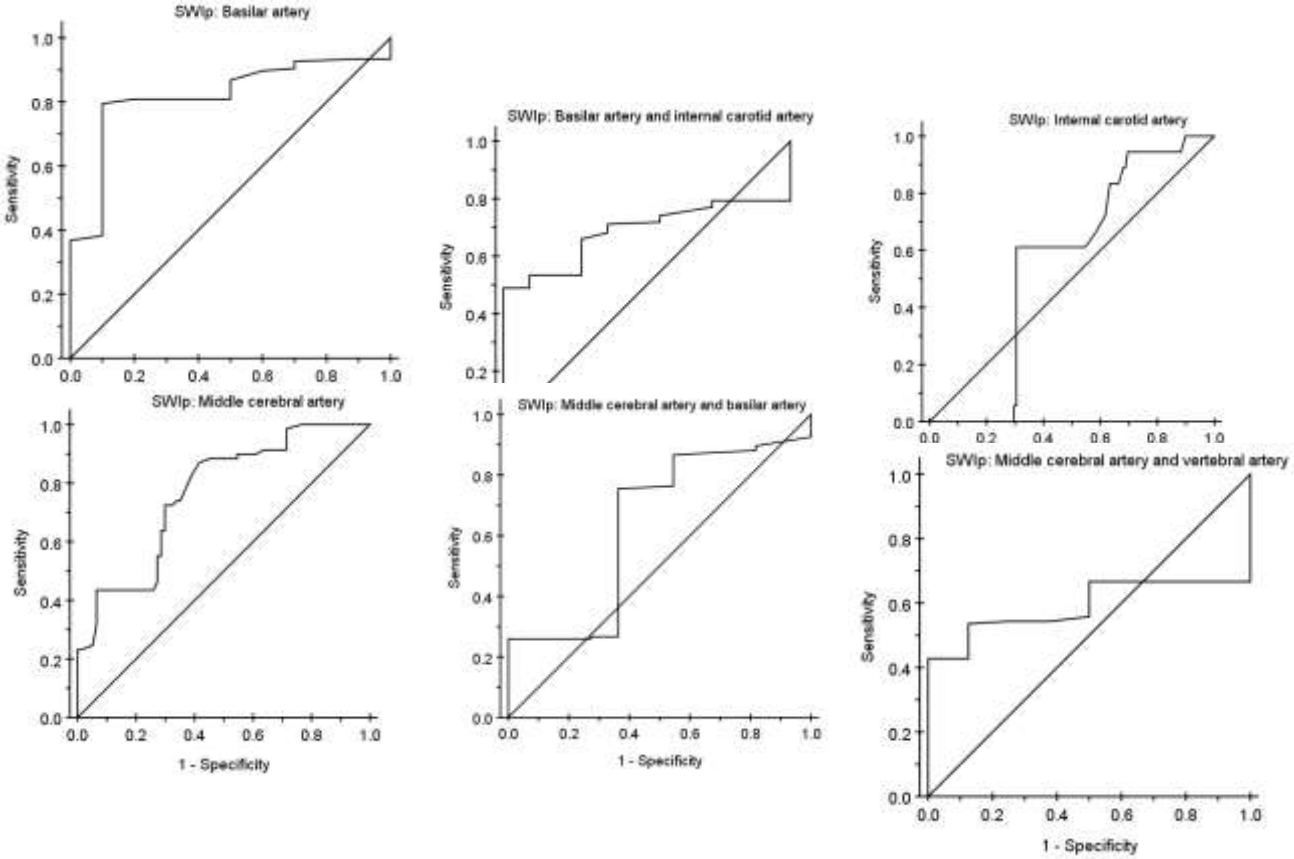

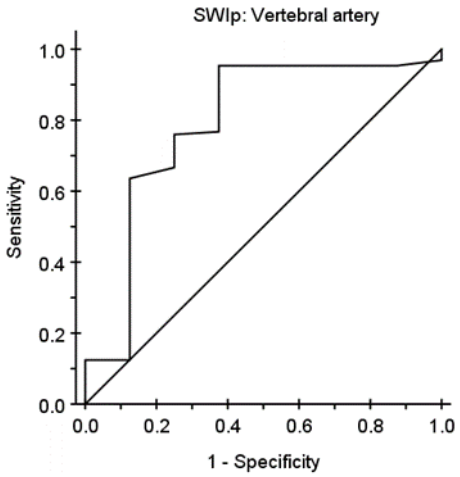

Figure 3.3: Receiver operating characteristic curve of susceptibility weighted imaging phase to identify intracranial arteries calcification. The 45° (reference) the line represents chance as a diagnostic criterion (AUC = 0.5).

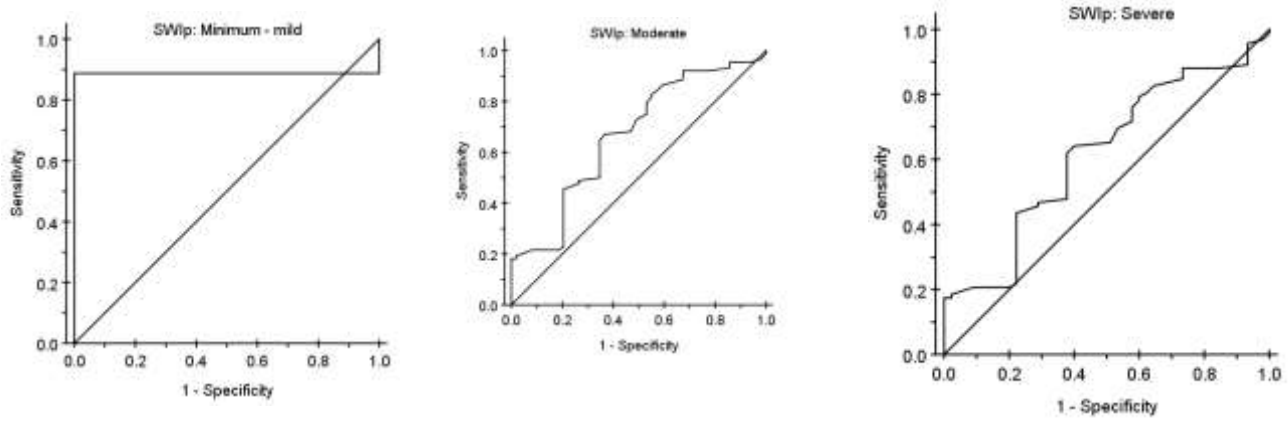

Figure 3.4: Receiver operating characteristic curve of susceptibility weighted imaging phase to identify intracranial arteries stenosis. The 45° (reference) the line represents chance as a diagnostic criterion (AUC = 0.5).

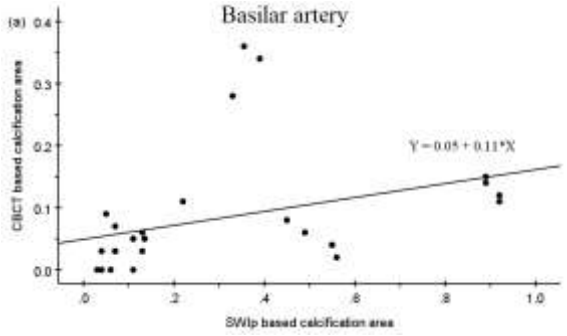
Basilar artery
(a)
CBCT based calcification area
SWIp based calcification area
Y = 0.05 + 0.11*X

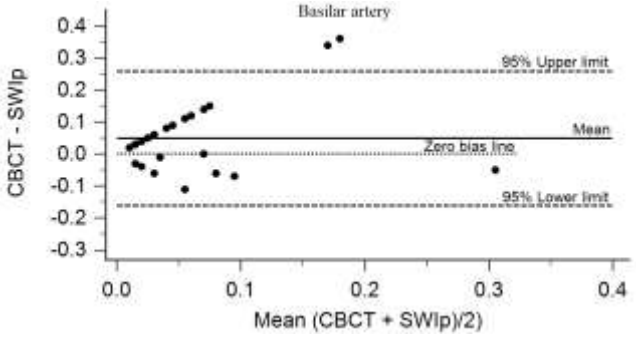
Basilar artery
95% Upper limit
Mean
Zero bias line
95% Lower limit
CBCT - SWIp
Mean (CBCT + SWIp)/2)

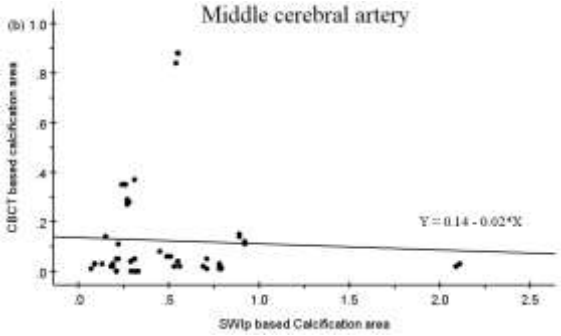
Middle cerebral artery
(b)
CBCT based calcification area
SWIp based Calcification area
Y = 0.14 - 0.02*X

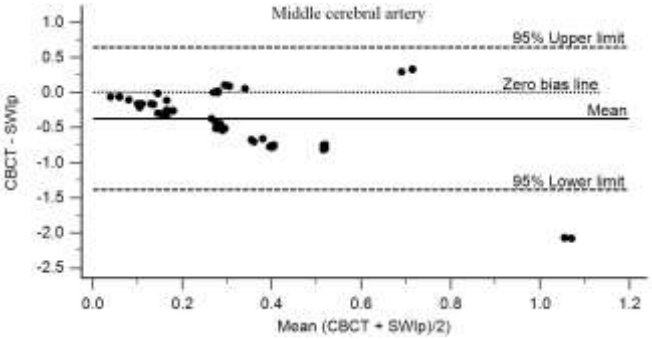
Middle cerebral artery
95% Upper limit
Zero bias line
Mean
95% Lower limit
CBCT - SWIp
Mean (CBCT + SWIp)/2)

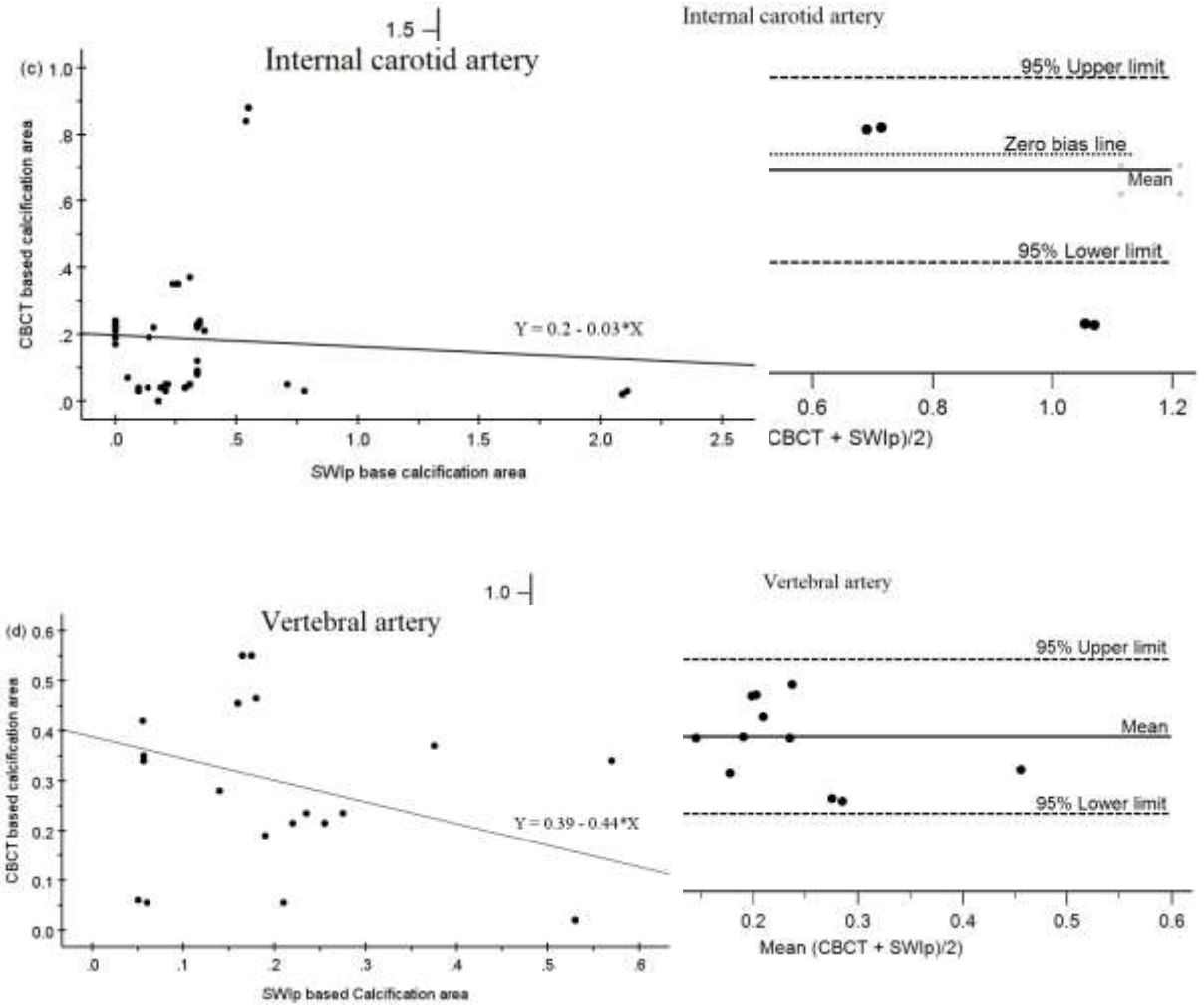
1.5
Internal carotid artery
(c) 1.0
.8
.6
.4
.2
.0
CBCT based calcification area
Y = 0.2 - 0.03*X
.0
.5
1.0
1.5
2.0
2.5
SWIp base calcification area
Internal carotid artery
95% Upper limit
Zero bias line
Mean
95% Lower limit
0.6
0.8
1.0
1.2
CBCT + SWIp)/2)
1.0
Vertebral artery
(d) 0.6
0.5
0.4
0.3
0.2
0.1
0.0
CBCT based calcification area
Y = 0.39 - 0.44*X
.0
.1
.2
.3
.4
.5
.6
SWIp based Calcification area
Vertebral artery
95% Upper limit
Mean
95% Lower limit
0.2
0.3
0.4
0.5
0.6
Mean (CBCT + SWIp)/2)

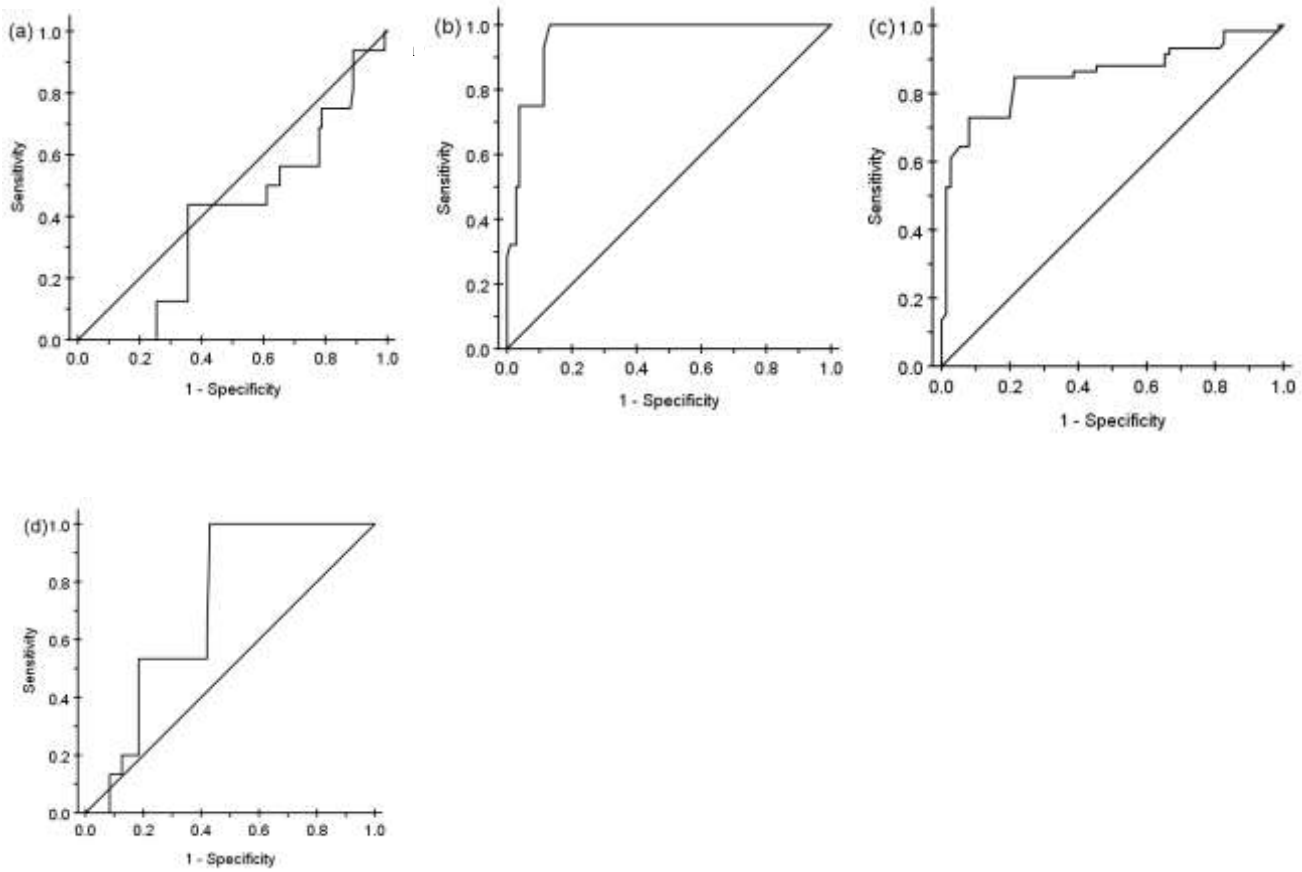

Figure 3.6: The discriminative power of susceptibility-weighted imaging phase to identify intracranial artery stenosis

(a) None Sens. = 100%, Spec. = 25%, Optimal cut-off value ≤ 845, AUC = 0.60 (0.51, 0.68), *P* = 0.177

(b) Min – mild intracranial calcium stenosis. Sens. = 100%, Spec. = 87%, Optimal cut-off value = ≤779, AUC = 0.96 (0.91, 0.98), *P* <0.001

(c) Moderate intracranial calcium stenosis. Sens. = 92%, Spec. = 73%, Optimal cut-off value ≤620, AUC = 0.85 (0.78, 0.91), *P* <0.001

(d) Severe intracranial calcium stenosis. Sens. = 100%, Spec. = 57%, Optimal cut-off value ≤524, AUC = 0.72 (0.64, 0.80), *P* <0.001

Discussion and Conclusion

The present study has several significant inferences about the ability of CBCT and SWIp to detect ICAD as well as the sensitivity, specificity, negative predictive value, positive predictive value, and predictive values of these modalities to detect ICAD from brain stroke patients attending Hospital Pengajar Universiti Putra Malaysia. The study was conducted within a space of two years; between January 2022 to December 2023.

In this study, intracranially, both CBCT and SWIp offered promising ability to detect and localize calcifications of intracranial arteries. In these populations, intracranial calcification is a risk factor for stroke, accounting for 128 (87.7%) as detected by CBCT angiography and 135 (92.5%) by SWI angiography in this group of stroke patients. The high prevalence of intracranial calcifications provides evidence that intracranial calcification, commonly used as a proxy for intracranial atherosclerosis is a major risk factor for stroke. In the present study, the prevalence is higher than the previously reported

prevalence of 40% in Korean patients (Sohn et al., 2004; Wu et al., 2016) and 69% of Chinese patients (Chen et al., 2006; De Silva et al., 2007). The higher prevalence in the present study than in the two previous studies may be due to the high sensitivity of CBCT and SWI modalities to the routine brain CT used in the Korean study and multi-detector-row computed tomography used in the Chinese study. It is worth acknowledging that the total burden of intracranial calcifications in this study comprises intracranial calcification in multiple intracranial arteries and not only the intracranial carotid arteries. Nevertheless, intracranial plaques in other cerebral arteries have been reported as typically noncalcified (Homburg et al., 2011; Sun et al., 2021). In the present study, contrast-enhanced CT was conducted to determine whether the high-density region was within the artery (calcification) or outside (bony structure).

In the present study, the severity of stenosis showed a significant association with the extent of calcifications. This result is consistent with other autopsy studies (Sollberg et al., 1968; Mathur et al., 1963). Thus, this implies that if the intracranial arteries are more calcified, there may also be an increased likelihood of atherosclerotic changes in the intracranial arteries. According to this theory, intracranial artery calcification serves as a signal for intracranial atherosclerosis overall. Nevertheless, calcification of the intracranial arteries may be a contributing factor to stroke.

Sometimes, the lumen of highly calcified vessels can become stenotic, which can cause hemodynamic problems (Woodcock et al., 1999). The remodeling (i.e., compensatory enlargement) of arteries makes this relationship complicated (Woodcock et al., 1999).

Based on CBCT angiography, the internal carotid artery has the highest prevalence of arterial wall calcifications (36.3%), followed by the anterior cerebral artery (3.4%), middle cerebral artery (9.6%), and vertebral artery (6.2%). The confluence of the vertebral artery and the basilar artery has the lowest prevalence (17.1%). The current study's findings were in line with those of the Korean study, which found that the internal carotid artery had the highest prevalence (Sohn et al., 2004). The prevalence of stenosis within the intracranial vessels was 74%. Intracerebral artery calcifications and stenosis were not shown to be significantly correlated. Subgroup analysis, however, revealed a moderately significant association between the grade of stenosis and internal carotid artery calcification ($r = 0.44$, $P = 0.022$, $n = 27$).

A patient's intracranial arterial profile and the choice and modification of their medical treatment may be greatly impacted by accurate and dependable imaging and diagnosis of intracranial artery calcification, given the mounting body of evidence (Bugnicourt et al., 2009; Faxon et al., 2004; Rennenberg et al., 2009) that links this condition to an increased risk of both fatal and non-fatal heart attacks and strokes. Comprehensive knowledge of vessel wall calcification of intracranial arteries of the central nervous system has been acknowledged as the basis of intracranial atherosclerosis. Globally, there is a significant prevalence of vessel wall calcification in the arteries that carry blood to the brain. Calcification of the blood-supplying arteries is a known characteristic of arteriosclerosis and could be a simple indicator of the severity of cerebrovascular illness (Pletcher et al., 2014). Recent research, including the extensive Rotterdam study, demonstrated intracranial vessel calcification as a significant stroke risk factor (Bos et al., 2014).

In this study, the prevalence of intracranial arterial calcification using CBCT and SWIp were respectively 87.7% and 92.5%. This indicates that SWIp is more powerful in identifying intracranial calcifications compared to CBCT. Considering CBCT, the internal carotid arteries showed the highest prevalence of intracranial arterial calcification (36.3%), while the middle cerebral artery showed the highest prevalence (47.3%) of calcification using the SWI technique. Variations in the incidence of internal carotid artery calcifications have been documented in earlier studies. The incidence of cerebral artery calcification in patients with acute cerebrovascular illness is between 40 and 87% (Koton et al., 2012). De Silva et al., (2007) reported a rate of 69% utilizing brain CT, whereas Chen et al. in 2019 observed a prevalence of internal carotid artery at 64.8% using both CT and MRI. Both studies were conducted among Chinese patients. The relatively lower prevalence noted in the present study might

have been caused by the difference in sample size as both CT and CBCT use the Agatston Scale to evaluate calcification automatically.

It has been reported that each internal carotid artery supplies ~40% of total perfusion to the brain (Kim et al., 2008; Kim et al., 2013). The high calcification rates (36.3%) of the internal carotid artery seen in this study may be associated with the high perfusion territory of this artery. The middle cerebral artery provides arterial blood supply to the largest magnitude of all the intracranial arterial circulation with the least variations compared to all the other intracranial arteries (Kim et al., 2008). The caliber of the middle cerebral artery has been reported to typically be 3/4 of the parent internal carotid artery (Gibo et al., 1981).

In the present study, the prevalence of intracranial calcification of the anterior cerebral artery was 3.4%. Intrinsic anterior cerebral artery calcification has been considered an uncommon cause of anterior cerebral artery territory infarction. In a study involving a set of 55 patients with anterior cerebral artery territory infarction, 10 had plausible cardiac embolization whereas only five had calcification primarily involving the anterior cerebral artery (Hou et al., 2022). Gacs et al. (1981) postulated the following pathways for stroke from a CT scan study: embolization, propagation of thrombotic material from an occluded internal carotid artery into the intracranial branches, and vasospasm or propagating thrombosis linked to the anterior communicating aneurysm. For this reason, they made no mention of intrinsic calcification caused by the anterior cerebral artery. Boguslavsky and Franco reported that of 27 patients with anterior cerebral artery, territory infarction embolism from the heart or internal carotid artery illness was observed in 17 patients (63%), whereas just one patient had in situ thrombotic blockage of the anterior cerebral artery.

However, research conducted in Asia produced remarkably different findings. According to Kazui et al., (1993), 17 Japanese patients underwent CT angiography evaluations. Only three patients (18%) experienced a cardiogenic infarction, while the bulk of patients (59%) were caused by intrinsic anterior cerebral artery calcification. A comparable outcome was found in a Korean investigation. Kang & Kim, (2008) examined a group of one hundred consecutive patients who had anterior cerebral artery territory infarction, as determined by MRI and angiography. Large artery calcification was the presumed cause in 73 cases, cardiogenic embolism in 10, large artery disease or cardiogenic embolism in two cases, and uncertain in 15 cases. Of the patients who had big artery calcification thrombosis, 61 had localized anterior cerebral artery atherosclerotic diseases, six had internal carotid artery diseases, and six had internal carotid artery diseases.

In several studies, sensitivity and specificity rates of CBCT and SWI were conducted, but such studies showed that CBCT is increasingly utilized in various medical imaging applications, including dentistry, orthodontics, and maxillofacial imaging here it offers advantages over traditional CT, such as lower radiation dose and higher spatial resolution (Zyoud et al., 2023). Whereas SWI is an advanced MRI technique that enhances the detection of subtle changes in tissue susceptibility, particularly for hemorrhagic lesions (such as microbleeds and larger hemorrhage), iron deposition, and calcification. However, in clinical practice, SWI is increasingly used to evaluate neurological conditions, such as traumatic brain injury, stroke, and vascular malformations (Zyoud et al., 2023).

The receiver operating characteristic curve analysis was used to assess the clinical validity of CBCT and SWI as diagnostic tools for detecting intracranial artery calcifications. The sensitivity, specificity, negative predictive value, and positive predictive value of the predictive values of CBCT and SWI for detecting intracranial artery calcifications were evaluated. The results of SWI were also compared with those of CBCT while maximizing the sensitivity and specificity (Elnekeidy et al., 2019). Cut-offs were derived for CBCT and SWI through ROC analysis to further improve the tradeoff between specificity and sensitivity. This study has demonstrated that both CBCT and SWI appeared to be useful diagnostic tools for detecting intracranial large artery calcium stenosis. The results revealed that both modalities have the same sensitivity (86%) to detect minimum – mild grade calcium score, while CBCT has relatively higher specificity (65%) compared to SWI (61%). The results show that the predictive values

of CBCT and SWI to detect minimum – mild stenosis were <0.17 mm2 and <0.39 mm2 respectively, and it was > 0.02 mm2 and <0.45 mm2 for moderate-grade stenosis. The sensitivity and specificity of CBCT were consistently higher for moderate and severe grade stenosis than SWI, signifying that CBCT can be more sensitive and specific for the diagnosis of all grades of large artery calcium stenosis than SWI.

4. Conclusion and future scope

In conclusion, in the present study, both susceptibility-weighted imaging (SWI) and cone-beam CT (CBCT) were effective for detecting intracranial calcifications in the basilar artery, each with its strengths. SWI excels in soft tissue contrast and safety (no ionizing radiation), while CBCT provides high spatial resolution and faster imaging times. The choice between the two modalities often depends on the specific clinical scenario, availability of equipment, and patient considerations. The findings of the present study provide evidence about the validity of CBCT and SWI as imaging techniques for diagnosing intracranial calcifications. Both CBCT and SWI provide a good predictive ability to detect intracranial vessel wall calcifications. Future studies should assess the sensitivity, and specificity and generate the predictive value of each grade of intracranial vessel stenosis of each intracranial artery rather than lumping all intracranial arteries together.

Reference

[1] Bang, O. Y. (2014). Intracranial Atherosclerosis: Current Understanding and Perspectives. *Journal of Stroke*, *16*(1), 27. https://doi.org/10.5853/jos.2014.16.1.27

[2] Bhatia, R., Sharma, G., Patel, C., Garg, A., Roy, A., Bali, P., Singh, N., Sisodia, P., Sreenivas, V., Srivastava, M. V. P., & Prasad, K. (2019). Coronary Artery Disease in Patients with Ischemic Stroke and TIA. *Journal of Stroke and Cerebrovascular Diseases*, *28*(12), 104400. https://doi.org/10.1016/j.jstrokecerebrovasdis.2019.104400

[3] Bos, D., Portegies, M. L. P., Van Der Lugt, A., Bos, M. J., Koudstaal, P. J., Hofman, A., Krestin, G. P., Franco, O. H., Vernooij, M. W., & Ikram, M. A. (2014). Intracranial carotid artery atherosclerosis and the risk of stroke in whites: The Rotterdam study. *JAMA Neurology*, *71*(4), 405–411. https://doi.org/10.1001/jamaneurol.2013.6223

[4] Bugnicourt, J. M., Garcia, P. Y., Peltier, J., Bonnaire, B., Picard, C., & Godefroy, O. (2009). Incomplete posterior circle of Willis: A risk factor for migraine?: Research submission. *Headache*, *49*(6), 879–886. https://doi.org/10.1111/j.1526-4610.2009.01389.x

[5] Chen, W., Zhu, W., Kovanlikaya, I., Kovanlikaya, A., Liu, T., Wang, S., Salustri, C., & Wang, Y. (2014). Intracranial calcifications and hemorrhages: Characterization with quantitative susceptibility mapping. *Radiology*, *270*(2), 496–505. https://doi.org/10.1148/radiol.13122640

[6] Chen, Y., Cai, J., & Jones, D. P. (2006). Mitochondrial thioredoxin in regulation of oxidant-induced cell death. *FEBS Letters*, *580*(28–29), 6596–6602. https://doi.org/10.1016/j.febslet.2006.11.007

[7] De Silva, D. A., Woon, F. P., Lee, M. P., Chen, C. P. L. H., Chang, H. M., & Wong, M. C. (2007). South Asian patients with ischemic stroke: Intracranial large arteries are the predominant site of disease. *Stroke*, *38*(9), 2592–2594. https://doi.org/10.1161/STROKEAHA.107.484584

[8] Elnekeidy, A. E., Yehia, A., Elfatatry, A., & Elnekeidy, A. E. (2019). Importance of susceptibility weighted imaging (SWI) in management of cerebrovascular strokes Importance of susceptibility weighted imaging (SWI) in management of cerebrovascular strokes (CVS). *Alexandria Journal of Medicine*, *50*(1), 83–91. https://doi.org/10.1016/j.ajme.2013.05.006

[9] Ezzeddine, M. A., Lev, M. H., Mcdonald, C. T., Rordorf, G., Oliveira-filho, J., Aksoy, F. G., Farkas, J., Segal, A. Z., Schwamm, L. H., Gonzalez, R. G., & Koroshetz, W. J. (2002). Added Clinical Value in the Assessment of Acute Stroke. *Stroke*, *33*, 959–967.

[10] Faxon, D. P., Creager, M. A., Smith, S. C., Pasternak, R. C., Olin, J. W., Bettmann, M. A., Criqui, M. H., Milani, R. V., Loscalzo, J., Kaufman, J. A., Jones, D. W., & Pearce, W. H. (2004). Atherosclerotic vascular disease conference: Executive summary: Atherosclerotic vascular disease conference proceeding for healthcare professionals from a special writing group of the American Heart Association. *Circulation*, *109*(21), 2595–2604. https://doi.org/10.1161/01.CIR.0000128517.52533.DB

[11] Gibo, H., Carver, C. C., Rhoton, A. L., Lenkey, C., & Mitchell, R. J. (1981). Microsurgical anatomy of the middle cerebral artery. *Journal of Neurosurgery*, *54*(2), 151–169. https://doi.org/10.3171/jns.1981.54.2.0151

[12] Homburg, P. J., Plas, G. J. J., Rozie, S., Van Der Lugt, A., & Dippel, D. W. J. (2011). Intracranial arterial stenotic lesions' prevalence and calcification were assessed with multidetector computed tomography angiography. *Stroke*, *42*(5), 1244–1250. https://doi.org/10.1161/STROKEAHA.110.596254

[13] Hou, D., Yang, X., Wang, Y., Huang, S., Tang, Y., & Wu, D. (2022). Carotid Siphon Calcification Predicts the Symptomatic Progression in Branch Artery Disease with Intracranial Artery Stenosis - Brief Report. *Arteriosclerosis, Thrombosis, and Vascular Biology*, *42*(8), 1094–1101. https://doi.org/10.1161/ATVBAHA.122.317670

[14] Jeng, J., Tang, S., & Liu, H. (2010). *Jeng2010*. 1423–1432.

[15] K., K. S. J. C. R. L. W. L. S. (2008). *Intracranial atherosclerosis. Blackwell Publishing Ltd.*

[16] Kamran, M. (2015). *Applications of novel imaging protocols and devices in interventional neuroradiology Oxford University, UK]*. (Vol. 34).

[17] Kang, S. Y., & Kim, J. S. (2008). Anterior cerebral artery infarction: stroke mechanism and clinical-imaging study in 100 patients. *Neurology*, *70*(24 Pt 2), 2386–2393. https://doi.org/10.1212/01.wnl.0000314686.94007.d0

[18] Kazui, S., Sawada, T., Naritomi, H., Kuriyama, Y., & Yamaguchi, T. (1993). Angiographic evaluation of brain infarction is limited to the anterior cerebral artery territory. *Stroke*, *24*(4), 549–553. https://doi.org/10.1161/01.STR.24.4.549

[19] Khan, M., Naqvi, I., Bansari, A., & Kamal, A. K. (2011). Intracranial atherosclerotic disease. *Stroke Research and Treatment*, *2011*(di). https://doi.org/10.4061/2011/282845

[20] Kim, H. S., Kim, D. M., Ju, C. Il, & Kim, S. W. (2013). Intracranial calcification caused by a brain abscess: A rare cause of intracranial calcification. *Journal of Korean Neurosurgical Society*, *54*(2), 148–150. https://doi.org/10.3340/jkns.2013.54.2.148

[21] Koton, S., Molshatzki, N., Bornstein, N. M., & Tanne, D. (2012). Low cholesterol, statins, and outcomes in patients with first-ever acute ischemic stroke. *Cerebrovascular Diseases*, *34*(3), 213–220. https://doi.org/10.1159/000342302

[22] Mark J. Pletcher, MD, MPH1, 2, Christopher T. Sibley, MD3, Michael Pignone, MD, MPH4, Eric Vittinghoff, PhD1, and Philip Greenland, M. (2014). Interpretation of the Coronary Artery Calcium Score in Combination with Conventional Cardiovascular Risk Factors: The Multi-Ethnic Study of Atherosclerosis (MESA). *Methods Enzymol.*, *538*(10), 151–169. https://doi.org/10.1161/CIRCULATIONAHA.113.002598.Interpretation

[23] Rennenberg, R. J. M. W., Kessels, A. G. H., Schurgers, L. J., Van Engelshoven, J. M. A., De Leeuw, P. W., & Kroon, A. A. (2009). Vascular calcifications as a marker of increased cardiovascular risk: A meta-analysis. *Vascular Health and Risk Management*, *5*, 185–197. https://doi.org/10.2147/vhrm.s4822

[24] S. Mittal, Wu, Z., & Neelavalli, J, E. M. H. (2009). PHYSICS REVIEW Susceptibility-Weighted Imaging : Technical Aspects and Clinical Applications, Part 2. *AJNR 30 兩*. https://doi.org/10.3174/ajnr.A1461

[25] Shin, J., Chung, J. W., Park, M. S., Lee, H., Cha, J., Seo, W. K., Kim, G. M., & Bang, O. Y. (2018). Outcomes after ischemic stroke caused by intracranial atherosclerosis vs dissection. *Neurology*, *91*(19), E1751–E1759. https://doi.org/10.1212/WNL.0000000000006459

[26] Sohn, Y. H., Cheon, H. Y., Jeon, P., & Kang, S. Y. (2004). Clinical implication of cerebral artery calcification on brain

CT. *Cerebrovascular Diseases*, *18*(4), 332–337. https://doi.org/10.1159/000080772

[27] Sun, B., Wang, L., Li, X., Zhang, J., Zhang, J., Liu, X., Wu, H., Mossa-Basha, M., Xu, J., Zhao, B., Zhao, H., Zhou, Y., & Zhu, C. (2021). Intracranial Atherosclerotic Plaque Characteristics and Burden Associated With Recurrent Acute Stroke: A 3D Quantitative Vessel Wall MRI Study. *Frontiers in Aging Neuroscience*, *13*(July), 1–13. https://doi.org/10.3389/fnagi.2021.706544

[28] Tan, K. S., & Venketasubramanian, N. (2022). Stroke Burden in Malaysia. *Cerebrovascular Diseases Extra*, *12*(2), 58–62. https://doi.org/10.1159/000524271

[29] Vinuela, G. G. A. . F. H. J. M. B. and F. . (1981). CT Visualization of Intracranial Arterial Thromboembolism. *Stroke*, *14*(5), 353–357.

[30] Woodcock, R. J., Goldstein, J. H., Kallmes, D. F., Cloft, H. J., & Phillips, C. D. (1999). Angiographic correlation of CT calcification in the carotid siphon. *American Journal of Neuroradiology*, *20*(3), 495–499.

[31] Wu, X. H., Chen, X. Y., Wang, L. J., & Wong, K. S. (2016). Intracranial artery calcification and its clinical significance. *Journal of Clinical Neurology (Korea)*, *12*(3), 253–261. https://doi.org/10.3988/jcn.2016.12.3.253

[32] Yaghi, S., Prabhakaran, S., Khatri, P., & Liebeskind, D. S. (2019). Intracranial Atherosclerotic Disease: Mechanisms and Therapeutic Implications. *Stroke*, *50*(5), 1286–1293. https://doi.org/10.1161/STROKEAHA.118.024147

[33] Zyoud, T. Y. T., Kabeer, A., Syafeeq, M., Noh, F., Binti, S., & Hamid, A. (2023). *A Mini Literature Review on the Application of Susceptibility Weighted Imaging in Neuroradiology A Mini Literature Review on the Application of Susceptibility Weighted Imaging in Neuroradiology*. *July*.

[34] Zyoud, T. Y. T., Kabeer, A., Syafeeq, M., Noh, F., Binti, S., Hamid, A., Nizam, S., Rashid, A., Suppiah, S., Perisamy, R. S., Tharek, A., & Rahim, E. A. (2023). *Mini Literature Review on the Classification of Intracranial Calcification and Cone Beam Computed Tomography Usefulness*. *56*(03), 881–885.